University of Nebraska - Lincoln
DigitalCommons@University of Nebraska - Lincoln

Anthony F. Starace Publications | Research Papers in Physics and Astronomy

10-1-2007

Attosecond pulse carrier-envelope phase effects on ionized electron momentum and energy distributions

Liang-You Peng
Peking University, Beijing

Anthony F. Starace
University of Nebraska-Lincoln, astarace1@unl.edu

Follow this and additional works at: http://digitalcommons.unl.edu/physicsstarace

Part of the Physics Commons

Peng, Liang-You and Starace, Anthony F., "Attosecond pulse carrier-envelope phase effects on ionized electron momentum and energy distributions" (2007). *Anthony F. Starace Publications.* Paper 106.
http://digitalcommons.unl.edu/physicsstarace/106

This Article is brought to you for free and open access by the Research Papers in Physics and Astronomy at DigitalCommons@University of Nebraska - Lincoln. It has been accepted for inclusion in Anthony F. Starace Publications by an authorized administrator of DigitalCommons@University of Nebraska - Lincoln.

Attosecond pulse carrier-envelope phase effects on ionized electron momentum and energy distributions

Liang-You Peng* and Anthony F. Starace
Department of Physics and Astronomy, The University of Nebraska, Lincoln, Nebraska 68588-0111, USA
(Received 3 May 2007; revised manuscript received 17 July 2007; published 1 October 2007)

We analyze carrier-envelope phase (CEP) effects on electron wave-packet momentum and energy spectra produced by one or two few-cycle attosecond xuv pulses. The few-cycle attosecond pulses are assumed to have arbitrary phases. We predict CEP effects on ionized electron wave-packet momentum distributions produced by attosecond pulses having durations comparable to those obtained by Sansone *et al.* [Science **314**, 443 (2006)]. The onset of significant CEP effects is predicted to occur for attosecond pulse field strengths close to those possible with current experimental capabilities. Our results are based on single-active-electron solutions of the three-dimensional, time-dependent Schrödinger equation including atomic potentials appropriate for the H and He atoms.

DOI: 10.1103/PhysRevA.76.043401 PACS number(s): 32.80.Rm, 42.65.Re, 32.80.Fb, 32.80.Qk

I. INTRODUCTION

Recently, Sansone *et al.* [1] reported the experimental realization of isolated, approximately single-cycle attosecond pulses with a pulse duration of about 130 as and a photon energy of about 36 eV. Particularly notable is that the carrier-envelope phase of their attosecond pulses was reported to be stable and capable of being tuned, such as by using aluminum foils of variable thickness [1]. As noted by these authors [1], "[t]he availability of single-cycle isolated attosecond pulses opens the way to a new regime in ultrafast physics, in which the strong-field electron dynamics in atoms and molecules is driven by the electric field of the attosecond pulses rather than by their intensity profile." Now that it has become possible experimentally to produce isolated few-cycle attosecond pulses in the xuv spectral regime with tunable carrier-envelope phases, we analyze in this work the carrier-envelope phase (CEP) effects that one may expect on momentum and energy distributions of electron wave packets produced by one or more such few-cycle attosecond xuv pulses.

Investigations of short-pulse laser-produced electron wave packets have a rather lengthy history in atomic, molecular, and optical (AMO) physics, although interest has most recently focused on those produced by xuv attosecond pulses. Electron wave packets have been studied extensively in Rydberg atoms (see, e.g., Refs. [2–5]), including recently those produced by ionizing Rydberg atoms with few-cycle rf pulses [6]. In the ps regime, interference between short-pulse laser-produced electron wave packets in the continuum has been studied theoretically for the case of H^- detachment in various combinations of external static electric and/or magnetic fields [7–9]. In the fs regime, interferences between photoelectron wave packets ionized from excited states of atomic potassium by pairs of time-delayed 30-fs Gaussian laser pulses were studied experimentally [10]. In addition, there were experimental demonstrations of the first CEP effects on photoelectron spatial distributions produced by 5-fs few-cycle laser pulses that were not initially phase stabilized [11] but later were phase stabilized [12] (see also [13] and references therein). In fact, since the late 1990s (see, e.g., [14–16]) there has been an explosion in both experimental and theoretical interest in CEP effects produced by sub-10-fs few-cycle laser pulses (see the recent reviews in [17,18] and references therein).

In the attosecond xuv pulse regime, both theory [19] and experiment [20,21] initially focused on using properties of the photoelectron wave packets produced by xuv pulses in the presence of an ir laser field to characterize the temporal structure of the attosecond pulses. Indeed, by 2005 the FROG-CRAB technique (i.e., frequency-resolved optical gating for complete reconstruction of attosecond bursts) was put forward as a means to completely characterize any kind of attosecond pulse or pulse train [22,23]. Conversely, analysis of the electron bursts produced by 250-as, 93-eV XUV pulses in the presence of a few-cycle IR laser field has been shown to allow the complete characterization of the ir laser field [24]. Very recently, the momentum-space interference patterns between electron wave packets produced by xuv attosecond pulse trains in the presence of a shearing ir laser field were investigated both experimentally and theoretically as a means to understand the xuv photoionization process as well as the dynamics of electron wave-packet motion in ir laser fields [25,26]. With regard to the dynamics of electron wave-packet motion in ir laser fields, two interesting theoretical proposals have recently been made. Ishikawa [27] has proposed controlling the interference between electron wave packets produced by two or three attosecond xuv pulses by means of the phase of a few-cycle ir laser pulse, thereby simulating a Young's double-or triple-slit interference experiment. Smirnova *et al.* [28] have proposed using an xuv attosecond pulse to probe the recollision electron wave packet produced and driven by an ir laser field. In all of these prior works, the xuv attosecond pulses are considered to have many cycles (i.e., CEP effects are not an issue). Also, when two or more xuv pulses are considered, they are generally assumed to be identical (except for a possible phase difference of π, as in the case of neighboring pulses in an attosecond pulse train).

*Present address: Key Laboratory for Mesoscopic Physics, Department of Physics, Peking University, Beijing 100871, China.

 ©2007 The American Physical Society

We analyze in this paper the effects of the CEP of a few-cycle attosecond xuv pulse as well as the relative phase of two such pulses on electron wave-packet momentum and energy distributions and their interference patterns. In Sec. II we give a brief description of our theoretical method, which is based on our recent work on the exact solution of the single-active-electron, three-dimensional, time-dependent Schrödinger equation for describing the ionization dynamics of atomic systems in strong laser fields [29]. In Sec. III A we analyze the effects of the CEP of a single few-cycle attosecond xuv pulse on the momentum and energy distributions of the ionized electron from both H and He atoms. In Sec. III B we consider the effects of the CEPs of two time-delayed few-cycle attosecond xuv pulses (with possibly different CEPs) on the momentum and energy distributions of the ionized electron wave packets. In Sec. IV we summarize and discuss our results and present some conclusions.

II. THEORETICAL FORMULATION

Our theoretical approach is based on our recent work on the direct solution of the full-dimensional, time-dependent Schrödinger equation (TDSE) for a single-electron atom in the presence of a strong laser pulse [29]. For the H atom, the atomic potential is simply the Coulomb field of the nucleus. For the He atom, we employ the effective one-electron potential given by Hartree [30], which has been used by others to model the He atom in strong laser fields [31].

For a neutral atom having a single active electron that is ionized by one or two attosecond pulses, the TDSE describing the active electron is given by

$$i\frac{\partial}{\partial t}\Psi(\mathbf{r},t) = [H_0(\mathbf{r}) + H_I(\mathbf{r},t)]\Psi(\mathbf{r},t), \tag{1}$$

where the field-free Hamiltonian H_0 is defined by

$$H_0 = -\frac{1}{2}\nabla^2 + V_C(r) = -\frac{1}{2}\left[\frac{1}{r^2}\frac{\partial}{\partial r}\left(r^2\frac{\partial}{\partial r}\right) - \frac{1}{r^2}\hat{L}^2\right] + V_C(r). \tag{2}$$

Here $\hat{L}^2$ is the square of the orbital angular momentum operator and $V_C(r)$ is the effective atomic potential, which has a long-range Coulomb tail. For the cases of H and He, $V_C(r)$ is given explicitly by

$$V_C(r) = \begin{cases} -\dfrac{1}{r}, & \text{for H}, \\ -\dfrac{1}{r}[1 + (1+\beta r/2)e^{-\beta r}], & \text{for He}, \end{cases} \tag{3}$$

where $\beta = 27/8$ [30].

The interaction of the active electron with one or more attosecond laser pulses is described in Eq. (1) by $H_I(\mathbf{r},t)$, which may be defined in either the length gauge or the velocity gauge. We adopt the velocity gauge in the present work, but we find that the results for the two gauges agree very well [in part since the potential $V_C(r)$ is local]. In the velocity gauge, $H_I(\mathbf{r},t)$ is given by

$$H_I(\mathbf{r},t) = -i\mathbf{A}(t)\cdot\boldsymbol{\nabla}, \tag{4}$$

where $\mathbf{A}(t)$ is the vector potential for the laser field. We consider the general case of two attosecond pulses, with frequencies ω_1 and ω_2 and intensities I_1 and I_2, with both assumed to be linearly polarized along the z axis. The vector potential for this two-pulse case is given by

$$\begin{aligned}\mathbf{A}(t) &\equiv A(t)\hat{\mathbf{z}} \\ &= A_1F_1(t)\sin\left[w_1\left(t+\frac{\tau_1}{2}\right)+\phi_1\right]\hat{\mathbf{z}} \\ &\quad + A_2F_2(t)\sin\left[w_2\left(t-T_d+\frac{\tau_2}{2}\right)+\phi_2\right]\hat{\mathbf{z}},\end{aligned} \tag{5}$$

where T_d is the time delay between the two pulses and $A_i = \sqrt{I_i/I_{\text{au}}}/\omega_i$ $(i=1,2)$, where $I_{\text{au}} = 3.51\times10^{16}\ \text{W/cm}^2$. The CEP is ϕ_i $(i=1,2)$, and the pulse duration is $\tau_i = n_iT_i$ (where $T_i = 2\pi/\omega_i$ is the period and n_i is the integer number of cycles in the ith attosecond pulse, $i=1,2$). The vector potential envelopes $F_1(t)$ and $F_2(t)$ are given by

$$F_1(t) = \begin{cases} \sin^2[\pi(t+\tau_1/2)/\tau_1], & |t| \leqslant \tau_1/2, \\ 0, & |t| > \tau_1/2, \end{cases} \tag{6}$$

and

$$F_2(t) = \begin{cases} \sin^2[\pi(t-T_d+\tau_2/2)/\tau_2], & |t-T_d| \leqslant \tau_2/2, \\ 0, & |t-T_d| > \tau_2/2, \end{cases} \tag{7}$$

respectively. The case in which only one attosecond pulse is present corresponds to setting $A_2=0$ in Eq. (5).

The angular part of the wave function in Eq. (1) may be treated analytically in the usual way—i.e., by employing the following expansion:

$$\Psi(\mathbf{r},t) \equiv \Psi(r,\theta,\phi,t) = \sum_{l=0}^{L}\sum_{m=-l}^{l}\frac{\varphi_{lm}(r,t)}{r}Y_{lm}(\theta,\phi). \tag{8}$$

The resulting Schrödinger equation for the radial coefficients can be solved using various different methods of discretizing the radial coordinate r [29]. For convenience in calculating the momentum-space wave function of the ionized electron, we choose the usual central finite-difference scheme with equal grid spacing—i.e., with radial grid points given by $r_i = i\Delta r$ where $i=1,2,\ldots,N_r$. To propagate the radial wave functions in time, we use the Arnoldi method. The atomic ground-state wave function is calculated by an imaginary-time propagation in the absence of the external field until the ground-state energy is fully converged.

After the end of the attosecond pulse(s), we continue propagating the electron's wave function until such time that the overlap of the ionized part with the initial state is insignificant. That is, we propagate for a sufficiently long time t_s so that the low-momentum components of the ionized part of the wave function reach a distance r_s that lies outside the region over which the initial-state wave function is significant. On the other hand, the radial box size $r_{\max} = N_r\Delta r$ must be chosen sufficiently large so that the high-momentum components of the ionized electron wave packet do not reach the

box edge before we terminate our time propagation. In this way, at the end of our time propagation the ionized electron wave function is located entirely between r_s and $r_{\max}$ (within our numerical accuracy). The momentum-space wave function may then be calculated by carrying out the Fourier transformation

$$\Upsilon(k,\theta',\phi') = \frac{1}{(2\pi)^{3/2}}\int_{r_s}^{r_{\max}} r^2 dr \int_0^{\pi} \sin\theta\, d\theta \times \int_0^{2\pi} d\phi\, \Psi(r,\theta,\phi,t_s) e^{-i\vec{k}\cdot\vec{r}}, \tag{9}$$

which simplifies to

$$\Upsilon(k,\theta',\phi') = \sum_{lm} (-i)^l Y_{lm}(\theta',\phi')\frac{1}{k} \times \int_{r_s}^{r_{\max}} \sqrt{kr} J_{l+1/2}(kr)\varphi_{lm}(r,t_s)dr, \tag{10}$$

upon substituting in Eq. (9) the usual plane-wave expansion

$$\exp[-i\vec{k}\cdot\vec{r}] = 4\pi\sum_{l=0}^{\infty}(-i)^l j_l(kr)\sum_{m=-l}^{m=l} Y_{lm}^*(\theta,\phi)Y_{lm}(\theta',\phi'), \tag{11}$$

carrying out the angular integrations analytically and making use of the definition $j_l(z)=\sqrt{\pi/2z}J_{l+1/2}(z)$.

Owing to the symmetry of k_x and k_y, we may set $k_y=0$ without loss of generality. The transition probability to the final state $(k_x,k_y=0,k_z)$ is calculated according to

$$P(k_x,k_z) = |\Upsilon(k_x,k_y=0,k_z)|^2 = P(E,\theta_k), \tag{12}$$

where $E=(k_x^2+k_z^2)/2$ and θ_k is the angle between the electron momentum $\mathbf{k}=(k_x,0,k_z)$ and the laser polarization axis $\hat{\mathbf{z}}$. The electron distributions in momentum and energy are normalized such that $\int_{-\infty}^{\infty}\int_{-\infty}^{\infty}P(k_x,k_z)dk_xdk_z \equiv \int_0^{\infty}\int_0^{2\pi}P(E,\theta_k)dEd\theta_k$.

The accuracy of our code has been verified by comparing our numerically calculated ground-state wave function for the H atom in both coordinate space and momentum space with the corresponding analytical results [32]. The agreement is excellent. Note that in using Eq. (10) to calculate the initial-state wave function in momentum space, one sets $r_s=\Delta r$. Other numerical aspects of our calculations are given below in Sec. III.

III. RESULTS AND DISCUSSION

In this section, we present and analyze electron wave-packet momentum and energy distributions for two different cases. In Sec. III A, we examine CEP effects of a single few-cycle attosecond pulse on the ionized electron momentum and energy distributions. In Sec. III B, we examine CEP effects on the ionized electron momentum and energy distributions for the case of two few-cycle attosecond pulses. In the latter case, we give an approximate formula for the energy positions of the interference minima originating from the overlap of the two electronic wave packets produced respectively by the two attosecond pulses.

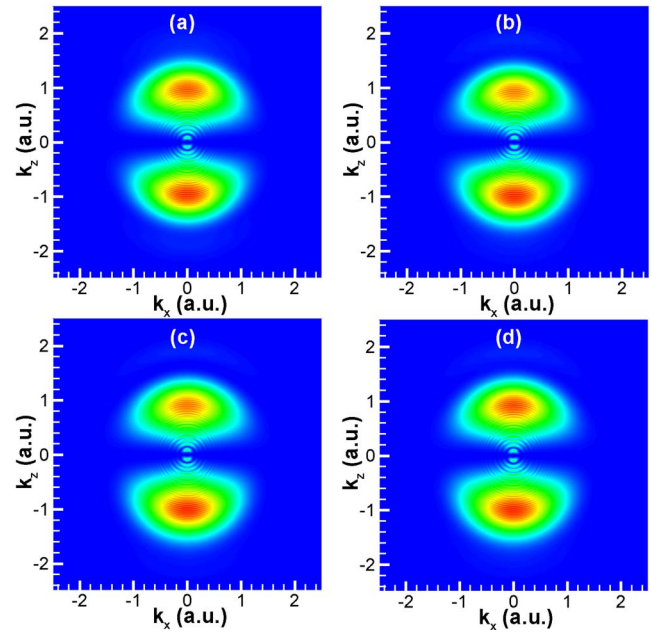

FIG. 1. (Color online) Momentum distributions of electrons ionized from He by a single few-cyle attosecond pulse with intensity $I_1=5\times10^{15}$ W cm^{-2}, frequency $\omega_1=1.32$ a.u., and pulse duration $\tau_1=2T_1$ for four different CEPs: (a) $\phi_1=0$, (b) $\phi_1=0.25\pi$, (c) $\phi_1=0.5\pi$, and (d) $\phi_1=0.75\pi$. The vector potentials of the corresponding attosecond pulses are shown in the insets in Fig. 2, where the electron energy distributions at the angles $\theta_k=0$ and $\theta_k=\pi$ are shown.

In all the calculations presented below, we use the following spatial and temporal parameters: all angular momenta in the range $0\leqslant l\leqslant 8$ are included, the radial grid spacing is $\Delta r=0.1$ a.u., the total number of radial grid points is $N_r=12\,000$, the time step for propagation is $\Delta t=0.01$ a.u., and the Arnoldi propagator is of order $M=30$. The starting point for the Fourier transformation in Eq. (10) for the final electronic wave function is taken to be $r_s=15$ a.u. Our results are fully converged with respect to all of these parameters. Furthermore, there is no reflection of the ionized electron wave packet from the box edge. Note that in Ref. [29] we defined a correction coefficient C_0 for the finite-difference representation of the second-order differential operator at the first grid point. In our present calculations for $\Delta r=0.1$ a.u., we have chosen $C_0=-1.221$ for both the H and He atom cases. The ground-state energies are calculated to be −0.5000 a.u. (−13.61 eV) for the H atom and −0.8875 a.u. (−24.15 eV) for the He atom [using the one-electron potentials in Eq. (3)]. The numerical result for H is thus exact, while that for He compares with the experimental value −24.59 eV.

A. CEP effects of a single few-cycle attosecond pulse

We demonstrate the effect of the CEP on electron momentum distributions ionized from He for the case of a single few-cycle (specifically, two cycle) attosecond pulse in Fig. 1. We have chosen the peak intensity $I_1=5\times10^{15}$ W cm^{-2} to be

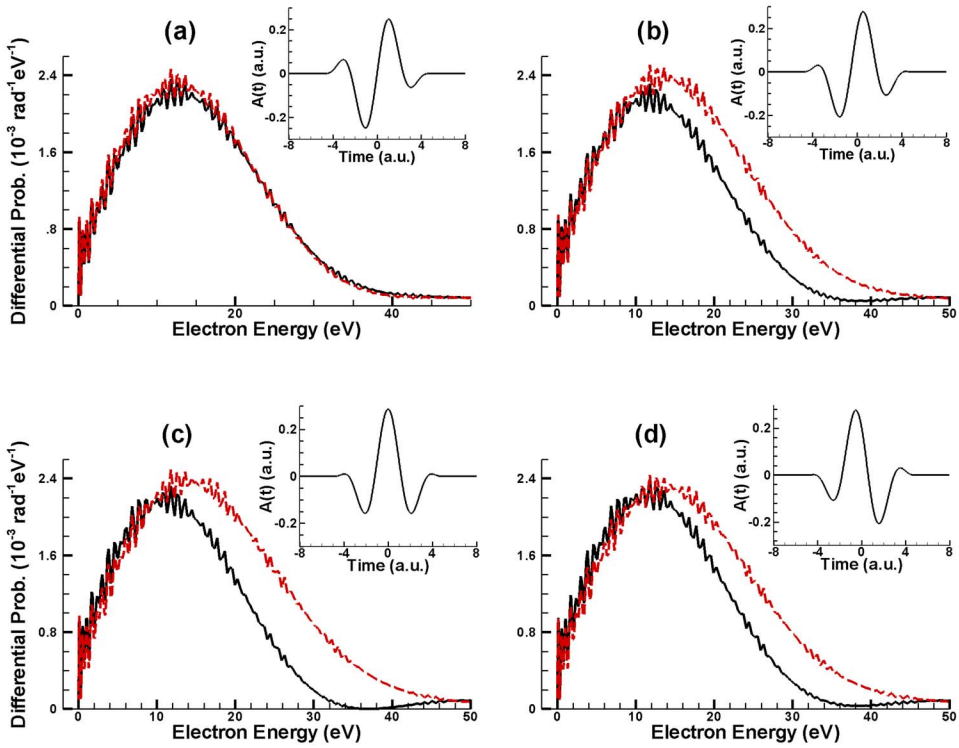

FIG. 2. (Color online) Energy distributions of electrons ionized from He by a single attosecond pulse with intensity $I_1=5\times10^{15}$ W cm^{-2}, frequency $\omega_1=1.32$ a.u., and pulse duration $\tau_1=2T_1$ at the angles $\theta_k=0$ (solid lines) and $\theta_k=\pi$ (dashed lines) relative to the direction of laser polarization. The CEPs of the pulses are (a) $\phi_1=0$, (b) $\phi_1=0.25\pi$, (c) $\phi_1=0.5\pi$, and (d) $\phi_1=0.75\pi$, respectively. The inset in each plot shows the corresponding vector potential of the attosecond pulse.

high enough so that the CEP effects are clearly visible. However, we emphasize that the asymmetry of the momentum and energy distributions resulting from the variation of the CEP of the pulse becomes significant at much lower peak intensities—e.g., at I_1 of the order of 10^{14} W cm^{-2}, which is experimentally feasible with good focusing of the attosecond pulse [33]. Besides the intensity, the other parameters of our single few-cycle attosecond pulse (given in the caption of Fig. 1) are similar to those achieved experimentally by Sansone *et al.* [1].

One sees from Fig. 1(a) that the ionized electron momentum distribution is asymmetric even for a CEP of zero. This is very different from the results of calculations employing the strong-field approximation (SFA), for which a symmetric distribution along the laser polarization direction is expected [18]. The asymmetry for $\phi_1=0$ may be due to Coulomb rescattering of lower-energy electrons, as has been found for few-cycle ir ionization of atoms [31,34,35]. Possible evidence of this rescattering is observable for small electron momenta in all panels of Fig. 1: the small ringlike features may originate from the interference of the rescattered portion of the ionized electron wave packet with the directly ionized electron wave packet. The largest asymmetry along the laser polarization direction is observed for a CEP of $\phi_1=0.5\pi$ [cf. Fig. 1(c)].

The asymmetry introduced by the CEP of the attosecond pulse becomes much clearer if one compares the electron energy distributions in the forward ($\theta_k=0$) and backward ($\theta_k=\pi$) directions. In Fig. 2, we show such energy distributions at the angles $\theta_k=0$ and $\theta_k=\pi$ for the four cases shown in Fig. 1. In Fig. 2(a), one observes that the energy distributions for the two angles are almost congruent with each other, except for differences in the small interference fringes that may be due to rescattering from the atomic potential. On the contrary, in Figs. 2(b)–2(d), one clearly observes an asymmetry in the energy distributions due to the CEP of the attosecond pulse. This asymmetry is observed both in the noticeable height difference of the two distributions and in the relative shift in energy between the distributions for these two ionization angles.

In Fig. 3, we exhibit the intensity dependence of these CEP-induced asymmetries in the ionized electron energy distributions and compare results for the He atom with those for the H atom. The energy distributions are shown for three different peak intensities I_1 and for the CEP giving the largest asymmetry $\phi_1=0.5\pi$. For the lowest peak intensity $I_1=5\times10^{13}$ W cm^{-2}, Figs. 3(a) and 3(d) show that there is little difference in the energy distributions in the two directions. As the intensity is increased, however, to 5×10^{14} W cm^{-2} [cf. Figs. 3(b) and 3(e)], differences in the energy distributions for the two directions become quite noticeable. At an intensity of 5×10^{15} W cm^{-2}, Figs. 3(c) and 3(f) show that the asymmetry in the energy distributions in the forward and backward directions becomes substantial. Compared with the results for the H atom, the results for the He atom exhibit much stronger interference fringes that may be due to the rescattering of low-energy electrons from the atomic potential. Also, the asymmetries in both the peak heights and the energy shifts of the electron energy distributions for He are much stronger than those in the distributions for H. These target differences originate from the stronger Coulomb potential at small distances experienced by low-energy electrons in He as well as the fact that the kinetic energies of electrons ionized from He are much smaller (i.e., on average, 11 eV smaller) owing to the larger ionization potential of the He ground state. Note finally that the probabilities for ionization from He at the photon energy of our

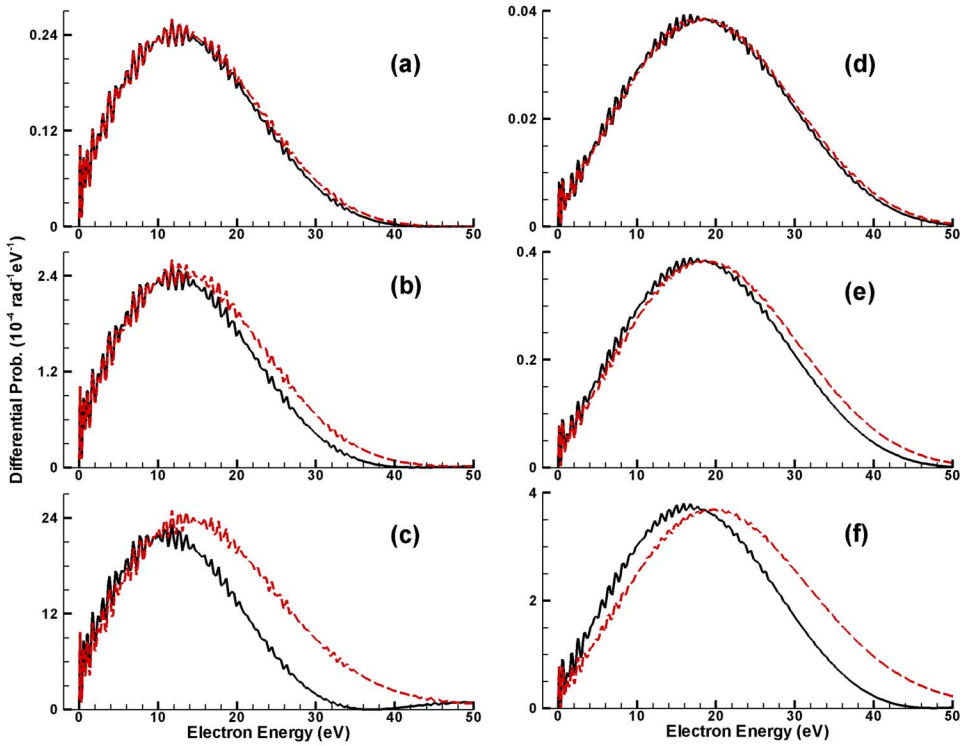

FIG. 3. (Color online) Comparisons of the electron energy distributions for He [(a),(b),(c)] and for H [(d),(e),(f)] ionized by a single attosecond pulse with frequency $\omega_1=1.32$ a.u., pulse duration $\tau_1=2T_1$, and CEP $\phi_1=0.5\pi$ for two ionization angles [$\theta_k=0$ (solid lines) and $\theta_k=\pi$ (dashed lines)] and three peak intensities, I_1 (in W cm^{-2}): 5×10^{13} [(a),(d)], 5×10^{14} [(b),(e)], and 5×10^{15} [(c),(f)].

xuv pulse are larger than those for ionization from H, in part owing to the fact that He has a two-electron ground state and in part owing to its larger one-electron dipole amplitude.

B. CEP effects of two attosecond pulses

In the case that there are two attosecond pulses instead of only one, it becomes possible to observe CEP effects in the interference between the two electronic wave packets produced by each pulse. This interference is exhibited in the electron momentum and energy distributions, provided that the frequencies ω_1 and ω_2, and the pulse durations τ_1 and τ_2, are such that the electron spectra produced by the two individual xuv pulses overlap in momentum. Denoting $f_1(E)$ and $f_2(E)$ to be the independent transition amplitudes for ionization by the first and second attosecond pulses respectively, the energy distribution produced by the two attosecond pulses applied in succession has the general form

$$P(E,\theta)=[f_1(E)e^{-i\Delta\Phi}+f_2(E)][f_1(E)e^{i\Delta\Phi}+f_2(E)]$$
$$=|f_1(E)|^2+|f_2(E)|^2+2|f_1(E)f_2(E)|\cos\Delta\Phi,$$

where $\Delta\Phi$ is the phase difference between the two electronic wave packets produced by the two attosecond pulses. The relative phase $\Delta\Phi$ comprises two parts: (i) the difference between the CEPs of the two attosecond pulses and (ii) the difference in the phase accumulation during the temporal evolution of the two electronic wave packets. Clearly, $f_i(E)$ $(i=1,2)$ depends on the electric field strength E_i and the dipole transition amplitude for the i*th* attosecond pulse.

In Fig. 4, we show the momentum distributions of electrons ionized from He by two attosecond pulses with frequencies $\omega_1=\omega_2=1.32$ a.u., pulse durations $\tau_1=\tau_2=2T_1$, and peak intensities $I_1=I_2=5\times10^{15}$ W cm^{-2} for three different pairs of CEPs. Since attosecond pulses are generally produced by a Ti:sapphire laser pulse, we take the time delay between the two attosecond pulses to be half a period of the Ti:sapphire laser, whose ir wavelength is 750 nm—i.e., $T_d=0.5T_{\rm ir}=51.71$ a.u. When the CEPs are zero—i.e., $\phi_1=\phi_2=0$—one observes in Fig. 4(a) that the interference fringes are symmetric (with respect to the direction of xuv laser polarization). However, the symmetry is broken when the CEP ϕ_2 is changed from 0 to 0.5π. Even greater asymmetry is observed in (c) when $\phi_1=\phi_2=0.5\pi$.

As we have done for the single-attosecond-pulse case, we compare in Figs. 5(a) and 5(b) the energy distributions of electrons ionized from the He atom and ejected parallel and anti-parallel to the z axis (i.e., the xuv pulse polarization axis) for two different pairs of xuv CEPs. These results correspond to the electron momentum distributions shown in Figs. 4(b) and 4(c), respectively. Similar energy spectra for electrons ionized from the H atom by the same pairs of attosecond pulses are shown in Figs. 6(a) and 6(b), respectively. Comparing Figs. 5 and 6, one sees clearly that the asymmetry in the peak heights at large energies for electrons ionized from He is much more significant than for electrons ionized from H. In contrast, the asymmetry in the peak heights at low energies for electrons ionized at the two different angles is insignificant in the case of He, but quite noticeable in the case of H. This may be due to the fact that the attraction between the ionized electron and the atomic potential is much more significant in the case of He than in the case of H, thus suppressing the effect of the CEP of the attosecond laser pulses in the case of He. In fact, this suppression in the asymmetry at low energies in the case of He as compared to H is observed as well in the case of a single attosecond pulse (cf. Fig. 3). Finally, we note that in Figs. 5 and 6 we have not included the case in which the CEPs of

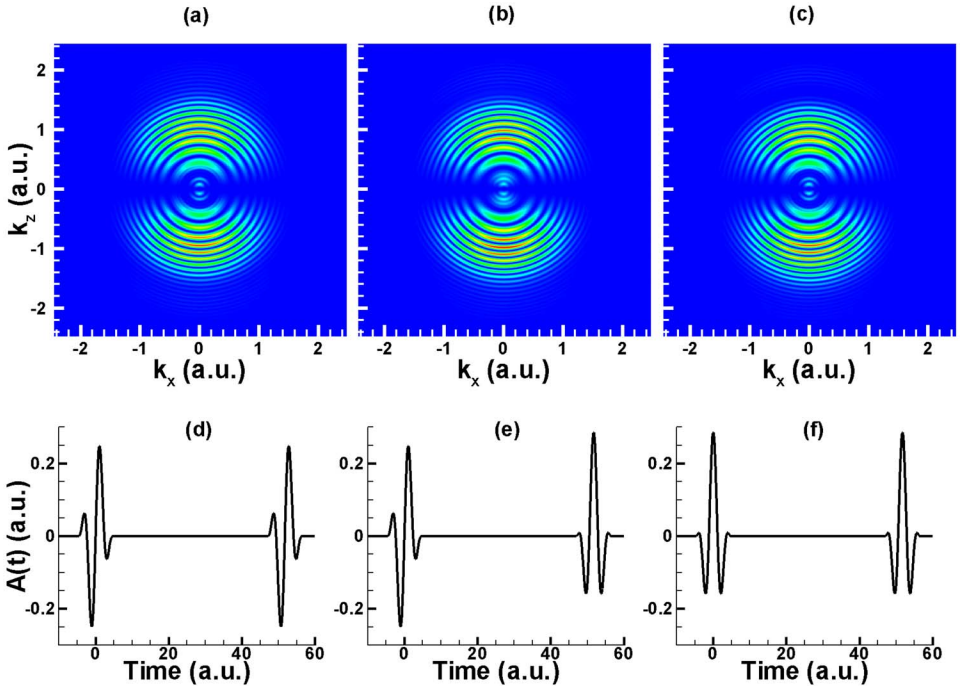

FIG. 4. (Color online) Momentum distributions of electrons ionized from He by two attosecond pulses with frequencies $\omega_1 = \omega_2 = 1.32$ a.u., pulse durations $\tau_1 = \tau_2 = 2T_1$, and peak intensities $I_1 = I_2 = 5 \times 10^{15}$ W cm^{-2} for different pairs of CEPs: (a) $\phi_1 = \phi_2 = 0$, (b) $\phi_1 = 0$, $\phi_2 = 0.5\pi$, and (c) $\phi_1 = \phi_2 = 0.5\pi$. The lower panels show the corresponding vector potentials of the two pulses in each case.

the two attosecond pulses differ by π. The reason is that the asymmetries in the electron energy distributions for electrons ionized parallel and antiparallel to the laser polarization axis are negligible in this case. One may "see" this by considering that the electron wave packets produced by each attosecond pulse individually are mirror images of each other with respect to $k_z = 0$ in the plane defined by k_z and k_x. (The tiny differences we do find in our calculations originate from the fact that the electron wave packet produced by the first attosecond pulse is affected slightly by the second attosecond pulse.)

Consider now the interference patterns observed in the energy distributions presented in Figs. 5 and 6. In order to understand these patterns, one needs to know the phase difference $\Delta\Phi$ in Eq. (13). In the simplest approximation, one may estimate this phase difference analytically if one neglects the interaction of the ionized electron with the atomic

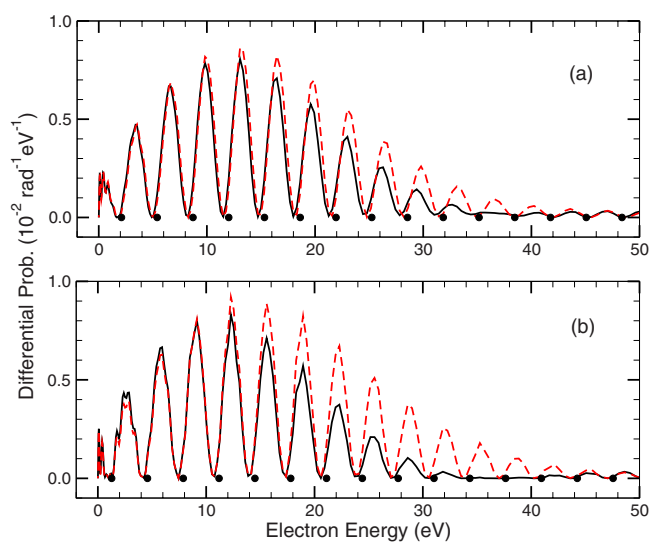

FIG. 5. (Color online) Comparisons of TDSE results for the energy distributions of electrons ionized from the He atom by two attosecond pulses at the angles $\theta_k = 0$ (solid lines) and $\theta_k = \pi$ (dashed lines). The frequencies, durations, and intensities of the two attosecond pulses are the same as those in Fig. 4. The CEPs are (a) $\phi_1 = 0$ and $\phi_2 = 0.5\pi$ and (b) $\phi_1 = 0.5\pi$ and $\phi_2 = 0.5\pi$. The solid circles indicate the predicted interference minimum positions according to the approximate Eq. (15). Note that the results in (a) and (b) correspond to those in Figs. 4(b) and 4(c), respectively.

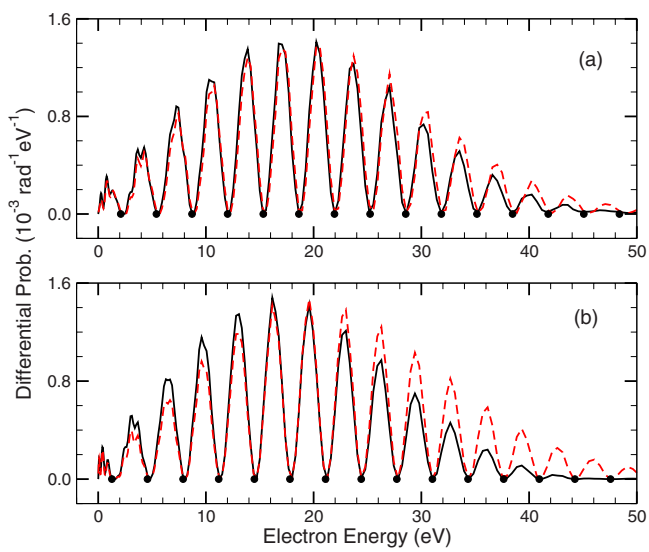

FIG. 6. (Color online) Comparisons of TDSE results for the energy distributions of electrons ionized from the H atom by two attosecond pulses at the angles $\theta_k = 0$ (solid lines) and $\theta_k = \pi$ (dashed lines). The frequencies, durations, and intensities of the two attosecond pulses are the same as those in Fig. 4. The CEPs are (a) $\phi_1 = 0$ and $\phi_2 = 0.5\pi$ and (b) $\phi_1 = 0.5\pi$ and $\phi_2 = 0.5\pi$. The solid circles indicate the predicted interference minimum positions according to the approximate equation (15).

potential. In this case, an electron with binding energy E_b that is ionized at time t_0 with a kinetic energy E by one of the attosecond pulses will evolve as a plane wave $[\propto e^{-i(E+E_b)(t-t_0)}]$. As noted above, the interference patterns between two electronic wave packets will be determined by the relative difference in their phases. If the two attosecond pulses have a difference in CEPs given by

$$\phi_{12} \equiv \phi_1 - \phi_2, \tag{13}$$

then the total phase difference $\Delta\Phi$ may be expressed as

$$\Delta\Phi = (E + E_b)T_d + \phi_{12}. \tag{14}$$

Note that in Eq. (14) we have neglected the phase accumulation correction of the first wave packet due to the vector potential of the second attosecond pulse owing to the latter's short temporal duration.

The interference minima in the energy spectra occur when $\Delta\Phi=(2n+1)\pi$ (where $n=0,\pm1,\pm2,\ldots$), which implies that

$$E_n^{\min} = -E_b + \frac{\pi}{T_d}\left(2n + 1 - \frac{\phi_{12}}{\pi}\right). \tag{15}$$

Note that this simple analytic prediction does not depend on the observation angle θ_k. Also, it predicts minima that are evenly spaced by $2\omega_{\rm ir}$ if $T_d=0.5T_{\rm ir}$. (Correspondingly, if one doubles the delay T_d, the spacing between minima will be halved to $\omega_{\rm ir}$.) More generally, experimental measurements of the interference pattern combined with this equation permit a determination of the time delay between the two attosecond pulses.

In Figs. 5 and 6, the positions of the minima in the energy spectrum predicted by the approximate formula in Eq. (15) are indicated as solid circles. One sees that the calculated energy positions of the interference minima agree very well with the predictions of Eq. (15) in the case of the H atom (cf. Fig. 6). In the case of He (cf. Fig. 5), the predicted minima lie higher in energy than given by the results of our exact solution of the TDSE, although the shift becomes smaller as the electron energy increases. This shift originates from our neglect of both the vector potential of the attosecond pulses and the atomic potential in deriving the approximate formula in Eq. (15).

General features of the interference minima predicted by the approximate formula in Eq. (15) are confirmed by our exact solutions of the TDSE. In particular, the positions of the interference minima do not depend on the angle θ and have a constant spacing of $2\pi/T_d$. Also, the positions of these minima only depend on the relative CEP ϕ_{12} between the two attosecond pulses, and not on the individual CEP values ϕ_1 and ϕ_2. This may be confirmed by comparing the He momentum distributions in Fig. 4, in which the positions of the minima are the same for the two pairs of CEPs shown in Figs. 4(a) and 4(c).

IV. SUMMARY AND DISCUSSION

In this work we have investigated the effects of the CEP of one or two attosecond pulses on ionized electron momentum and energy distributions. Now that single few-cycle attosecond pulses with well-defined and controllable CEPs have been achieved experimentally [1], it remains to determine what CEP effects there are and, most importantly, at what intensity these effects may be experimentally observable. In this work, we find that CEP effects on ionized electron momentum and energy distributions become visible at intensities of the order of 10^{14} W cm^{-2} and become clearly visible for intensities of the order of 10^{15} W cm^{-2}. According to Kienberger [33], with current technology it is probably possible to produce attosecond pulses having an intensity of order 10^{14} W cm^{-2}. Thus the effects predicted here may be amenable to experimental measurement.

In any experiment involving a few-cycle laser pulse, the electric field of the laser pulse will experience a phase change of π (i.e., the so-called Gouy phase) when passing through the laser focus [36]. This phase change occurs over a distance given by twice the Rayleigh length, which becomes smaller the more tightly one focuses the laser pulses [36]. However, a key parameter for any experimental measurement of CEP effects is the ratio of the atomic beamwidth to the Rayleigh length. If this ratio is small, then the effect of the Guoy phase on the results will be correspondingly small. In addition, the CEP effects predicted here are clearly such that they can be observed despite phase changes in a particular experiment originating from the Guoy phase. Indeed, as may be seen in Fig. 2, the CEP asymmetry effects we predict persist over a range of CEPs of π: i.e., the energy distributions at the angle $\theta_k=\pi$ all have a positive energy shift relative to those at the angle $\theta_k=0$ for all three of the CEPs shown, which lie in the range $0<\phi<\pi$. This fact, plus the experimental ability to fix the ratio of the atomic beam width to the Rayleigh length, augurs well for the feasibility of measuring the attosecond CEP effects predicted here.

As this work shows, the CEP of an attosecond pulse provides an additional tool with which researchers can control electron dynamics in atomic and molecular processes initiated or influenced by few-cycle attosecond pulses. Based on the present results, attosecond pulse CEP effects on ionized electrons in the presence of an additional IR laser field may also be expected to be significant. Such processes are currently under investigation.

ACKNOWLEDGMENTS

The authors thank Reinhard Kienberger for providing details on his experiments and on current experimental capabilities. One of us (A.F.S.) also thanks Philippe Antoine and Marc Vrakking for helpful discussions concerning experimental aspects related to this research. This work was supported in part by the Department of Energy, Office of Science, Division of Chemical Sciences, Geosciences, and Biosciences under Grant No. DE-FG02-96ER14646.

[1] G. Sansone, E. Benedetti, F. Calegari, C. Vozzi, L. Avaldi, R. Flammini, L. Poletto, P. Villoresi, C. Altucci, R. Velotta, S. Stagira, S. De Silverstri, and M. Nisoli, Science **314**, 443 (2006).
[2] G. Alber and P. Zoller, Phys. Rep. **199**, 231 (1991).
[3] G. Alber, H. Ritsch, and P. Zoller, Phys. Rev. A **34**, 1058 (1986).
[4] L. D. Noordam, D. I. Duncan, and T. F. Gallagher, Phys. Rev. A **45**, 4734 (1992).
[5] T. C. Weinacht, J. Ahn, and P. H. Bucksbaum, Phys. Rev. Lett. **80**, 5508 (1998).
[6] A. Gürtler, F. Robicheaux, W. J. van der Zande, and L. D. Noordam, Phys. Rev. Lett. **92**, 033002 (2004).
[7] Q. Wang and A. F. Starace, Phys. Rev. A **48**, R1741 (1993).
[8] Q. Wang and A. F. Starace, Phys. Rev. A **51**, 1260 (1995).
[9] L.-Y. Peng, Q. Wang, and A. F. Starace, Phys. Rev. A **74**, 023402 (2006).
[10] M. Wollenhaupt, A. Assion, D. Liese, Ch. Sarpe-Tudoran, T. Baumert, S. Zamith, M. A. Bouchene, B. Girard, A. Flettner, U. Weichmann, and G. Gerber, Phys. Rev. Lett. **89**, 173001 (2002).
[11] G. G. Paulus, F. Grasbon, H. Walther, P. Villorese, M. Nisoli, S. Stagira, E. Priori, and S. De Silvestri, Nature (London) **414**, 182 (2001).
[12] G. G. Paulus, F. Lindner, H. Walther, A. Baltuška, E. Goulielmakis, M. Lezius, and F. Krausz, Phys. Rev. Lett. **91**, 253004 (2003).
[13] A. J. Verhoef, A. Fernández, M. Lezius, K. O'Keefe, M. Uiberacker, and F. Krausz, Opt. Lett. **31**, 3520 (2006).
[14] E. Cormier and P. Lambropoulos, Eur. Phys. J. D **2**, 15 (1998).
[15] A. de Bohan, P. Antoine, D. B. Milošević, and B. Piraux, Phys. Rev. Lett. **81**, 1837 (1998).
[16] I. P. Christov, Opt. Lett. **24**, 1425 (1999).
[17] T. Brabec and F. Krausz, Rev. Mod. Phys. **72**, 545 (2000).
[18] D. B. Milošević, G. G. Paulus, D. Bauer, and W. Becker, J. Phys. B **39**, R203 (2006).
[19] M. Kitzler, N. Milosevic, A. Scrinzi, F. Krausz, and T. Brabec, Phys. Rev. Lett. **88**, 173904 (2002).
[20] F. Quéré, J. Itatani, G. L. Yudin, and P. B. Corkum, Phys. Rev. Lett. **90**, 073902 (2003).
[21] S. A. Aseyev, Y. Ni, L. J. Frasinski, H. G. Muller, and M. J. J. Vrakking, Phys. Rev. Lett. **91**, 223902 (2003).
[22] F. Quéré, Y. Mairesse, and J. Itatani, J. Mod. Opt. **52**, 339 (2005).
[23] Y. Mairesse and F. Quéré, Phys. Rev. A **71**, 011401(R) (2005).
[24] E. Goulielmakis, M. Uiberacker, R. Kienberger, A. Baltuska, V. Yakovlev, A. Scrinzi, Th. Westerwalbesloh, U. Kleineberg, U. Heinzmann, M. Drescher, and F. Krausz, Science **305**, 1267 (2004).
[25] T. Remetter, P. Johnsson, J. Mauritsson, K. Varjú, Y. Ni, F. Lépine, E. Gustafsson, M. Kling, J. Kahn, R. López-Martens, K. J. Schafer, M. J. J. Vrakking, and A. L'Huillier, Nat. Phys. **2**, 323 (2006).
[26] K. Varjú, P. Johnsson, J. Mauritsson, T. Remetter, T. Ruchon, Y. Ni, F. Lépine, M. Kling, J. Kahn, K. J. Schafer, M. J. J. Vrakking, and A. L'Huillier, J. Phys. B **39**, 3983 (2006).
[27] K. L. Ishikawa, Phys. Rev. A **74**, 023806 (2006).
[28] O. Smirnova, S. Patchkovskii, and M. Spanner, Phys. Rev. Lett. **98**, 123001 (2007).
[29] L.-Y. Peng and A. F. Starace, J. Chem. Phys. **125**, 154311 (2006).
[30] D. R. Hartree, *The Calculation of Atomic Structures* (Wiley, New York, 1957), Sec. 2.5.
[31] S. Chelkowski, A. D. Bandrauk, and A. Apolonski, Phys. Rev. A **70**, 013815 (2004).
[32] H. A. Bethe and E. E. Salpeter, *Quantum Mechanics of One- and Two-Electron Atoms* (Springer-Verlag, Berlin, 1957), p. 39.
[33] R. Kienberger (private communication).
[34] S. Chelkowski and A. D. Bandrauk, Phys. Rev. A **65**, 061802(R) (2002).
[35] D. B. Milošević, G. G. Paulus, and W. Becker, Opt. Express **11**, 1418 (2003).
[36] F. Lindner, G. G. Paulus, H. Walther, A. Baltuska, E. Goulielmakis, M. Lezius, and F. Krausz, Phys. Rev. Lett. **92**, 113001 (2004).